Study of Tidal Dynamics, Wetland Hydrology and Permafrost Degradation Using ALOS PALSAR Interferometry

ALOS PI No. 226
Principal Investigator: C.K. Shum[(1)]
Co-Investigators: Sangho Baek[(2)]**, Alexander Braun**[(3)]**, Michael Bäßler**[(4)]**,**
Reinhard Dietrich[(4)]**, Jimwoo Kim**[(1)]**, Hyongki Lee**[(1)]**, Zhong Lu**[(3)]

[(1)] School of Earth Sciences, Ohio State University, USA, ckshum@osu.edu
[(2)] Dept. of Civil Engineering & Environmental Science, Korea Military Academy, Korea, shark@kma.ac.kr
[(3)] Department of GeosciencesGeomatics Engineering, University of Texas at Dallas, USA, braun@utdallas.edu
[(4)] Institut für Planetare Geodäsie, Technische Universität Dresden, Germany,
baessler@IPG.geo.tu-dresden.de, dietrich@ipg.geo.tu-dresden.de
[(5)] EROS Center & Cascades Volcano Observatory, United States Geological Survey, USA, lu@usgs.gov

SUMMARY

The knowledge of ocean tides underneath permanently or seasonally sea ice covered ocean and ice shelves over Antarctica, is poorly known at fine-spatial scales. Significant amount of West Antarctic ice sheet melt is through the mechanism of basal melting and due to turbulent tidal mixing. We originally proposed to use the ALOS L-band PALSAR to model ocean tides underneath Antarctic ice-shelves. However, due primariy to its long repeat-orbits of 46-days, we are largely unsuccessful to construct coherent interferograms over the Filchner Ronne Ice Shelf (FRIS) using ALOS PALSAR. As a result we conducted a study using ERS-1/-2 tandem mission data to demonstrate the estimation of O_1 tides over the Sulzberger ice shelf, Ross Sea, West Antarctica. We used ALOS along with satellite radar altimetry as vertical reference to construct high-resolution (~40 m) water level changes in vegetated wetlands, including Louisiana, Helmand River, Amazon wetland, and the St. Clair Flats wetland in the Great Lakes. We also demonstrated the use of ALOS PALSAR to measure permafrost surface subsidence over the Tibetan Plateau, and thus inferring its Active Layer Thickness (ALT) change.

Keywords: SAR interferometry, ocean tides, wetland hydrology, permafrost

1. ICE SHELF DEM & OCEAN TIDE MODELING

Here we describe a demonstration of the feasibility of fine spatial scale (as fine as 100 m or less) O_1 barotropic ocean tide modeling underneath the Sulzberger ice shelf, Ross Sea, West Antarctica, using the VV-polarized C-band ERS-1/-2 tandem mission two-pass SAR interferometry time series [*Baek*, 2006; *Shum et al.*, 2007, 2008, 2009; *Baek et al.*, 2011]. The tidal inversion is accomplished by first developing a 60-m resolution DEM over the ground ice and the adjacent ice shelves using ERS tandem InSAR and ICESat altimetry, thereby diminishing the stringent data requirement in four-pass InSAR [*Kwoun et al.*, 2005; *Baek et al.*, 2006], and generate an InSAR (projected to height changes) time series for tidal analysis [*Baek*, 2006; *Baek et al.*, 2011]. Differential interferograms from the ERS-1/ERS-2 tandem mission SAR scenes acquired in the austral fall of 1996 are used together with four selected ICESat laser altimetry profiles in the austral fall of 2004 which provides GCPs, resulting in an improved geocentric 60-m resolution DEM over the grounded ice region. The InSAR DEM is then extended to include two ice tongues using ICESat profiles via kriging. Fourteen additional ICESat profiles acquired in 2003-2004 are used to assess the accuracy of the DEM. After accounting for radar penetration depth and predicted surface changes, including effects due to ice mass balance, solid Earth tides, and glacial isostatic adjustment, in part to account for the eight-year data acquisition discrepancy, the resulting difference between the DEM and ICESat profiles is –0.55±5.46 m. After removing the discrepancy between the DEM and ICESat profiles for a final combined DEM using a bicubic spline, the overall difference is 0.05±1.35 m indicating excellent consistency.

An O_1 ocean tide model is estimated using the InSAR height change time series after applying solid Earth tide correction, and the inverted barometric correction using the ECMWF pressure fields over the Sulzberger ice shelf. We examined ALOS PALSAR data availability over the Filchner Ronne Ice Shelf (FRIS) and have ordered data to attempt to generate interferograms to study the feasibility of using PALSAR to enhance ice shelf ocean tide modeling. However, our attempt was unsuccessful primarily because of the relatively long SAR scene repeating interval of 46 days.

The following section describes the details of ocean tide modeling over Sulzberger ice shelf using ERS-1/-2

tandem mission two-pass SAR interferometry.

1.1 Tidal Modeling Observational Equation

The phase information in an interferogram consists of topography and deformation signals. To assess the vertical deformation from an interferogram, first, an InSAR DEM is generated, as described in the previous section, but by averaging two DEMs and with corrected topography signals. The ocean tidal signal can be expressed as a function of time, t, and location (ϕ, λ) as follows:

$$\zeta(t,\phi,\lambda) = a + b\cdot t + \sum_{i=1}^{n} f_i H_i(\phi,\lambda)\cos(\omega_i t + \Theta_i(t_0) + \chi_i + u_i - G_i(\phi,\lambda)) \quad (1)$$

where ω_i is the angular frequency for the tidal constituent *i*; *t* is Universal Time measured in mean solar days from a reference epoch t_0 such as January 1, 0h.000, 1900; $\Theta_i(t_0)$ is the astronomical argument at t_0; $H_i(\phi,\lambda)$ and $G_i(\phi,\lambda)$ are the amplitude and phase for the tidal constituent i at location (ϕ,λ); χ_i is the additive phase correction; f_i and u_i are slowly varying functions to account for the longitude of the lunar node. The observation from InSAR is the range difference ΔR along the line of sight between times t_1 and t_2 such as $\Delta R = R(t_1,\varphi,\lambda) - R(t_2,\varphi,\lambda)$ and is converted to the surface elevation change to form an observation equation:

$$\Delta\zeta(t_1,t_2,\phi,\lambda) = \zeta(t_1,\phi,\lambda) - \zeta(t_2,\phi,\lambda) = b(t_1 - t_2) + \sum_{i=1}^{n}[C_i(\phi,\lambda)(\cos\Omega_{i,1} - \cos\Omega_{i,2}) + S_i(\phi,\lambda)(\sin\Omega_{i,1} - \sin\Omega_{i,2})] \quad (2)$$

where the harmonic coefficients $C_i(\phi,\lambda)$ and $S_i(\phi,\lambda)$ are defined as:

$$C_i(\phi,\lambda) = f_i H_i(\phi,\lambda)\cos G_i(\phi,\lambda) \quad (3)$$

$$S_i(\phi,\lambda) = f_i H_i(\phi,\lambda)\sin G_i(\phi,\lambda) \quad (4)$$

Amplitude and phase are computed by the harmonic coefficients as follows:

$$H_i(\phi,\lambda) = \frac{\sqrt{C_i^2(\phi,\lambda) + S_i^2(\phi,\lambda)}}{f_i} \quad (5)$$

$$G_i(\phi,\lambda) = \arctan\left(\frac{S_i(\phi,\lambda)}{C_i(\phi,\lambda)}\right) \quad (6)$$

1.2 Fine-Resolution Ice Shelf Ocean Tide Modeling

K_1 and O_1 are dominant constituents for Sulzberger glacier f_{K1}=1.0027/day, f_{O1}=0.9295/day, respectively. Due to the ERS orbital characteristics, the K_1 signal is diminished in the interferogram time series, and we have estimated the O_1 tide solution with a spatial resolution of 200 m by 200 m over the Sulzberger glacier. Fig. 1 shows the resulting amplitude and phase of the O_1 tides, and their corresponding errors [*Baek et al.*, 2011]. Table 1 shows the amplitude and phase and their uncertainties of two points, at the center and edge of the ice shelf, respectively [*Baek et al.*, 2011].

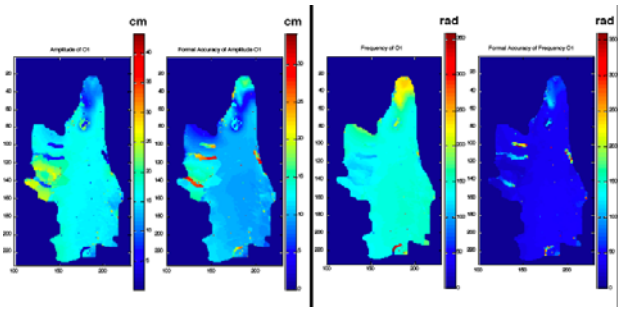

Figure 1. ERS-1/-2 InSAR derived 200-m Resolution O_1 Ocean Tide Model (Amplitude and Error, Phase and Error, left to right) Over the Sulzberger Glacier, W. Antarctica.

Location	Amplitude, cm	rms error, ±cm	Phase, deg	rms error, ±deg
Edge	17.4	7.8	155.7	34.8
Center	17.1	7.2	155.6	32.7

Table 1. O_1 Tides at the Ice Center & Edge of the Ice Shelf

1.3 ALOS PALSAR Data Processing

We describe our effort to order and process ALOS PALSAR over the FRIS towards building a time series adequate for InSAR ocean tide modeling. To generate tide modeling, an accumulated times series over a certain spot or limited area is necessary. The certain spot or area is again limited to across the grounding line where the ice contacted to the ground meets ocean under it. To solve at least a couple of tidal constituents from tidal difference equation given in equation (2), six or more revisiting time series are required. Unfortunately, however, ALOS in the very early stage of its mission period, data accumulation over across the grounding line. Fig. 3 shows that there is no available ALOS PALSAR FBS (Fine Beam Standard) mode level-0 data over FRIS. Fig. 4 shows an enlarged region (red circle in Figure 3) of the ice shelf and the data masks.

Only available data from Alaska Satellite Facility (ASF) ordering site was depicted in Fig. 5. On orbit number 5080, granules between 5460 and 5470 are the only available data satisfying location requirement that is near grounding line. However, the data was not processed successfully because the first frame of each acquisition contains some pre-acquisition calibration data, which cannot be processed which means the data is calibration scene. As a result, our first attempt is unsuccessful and

we are still waiting for ALOS PALSAR data over major Antarctic ice shelves including FRIS and Ross Ice Shelf (RIS).

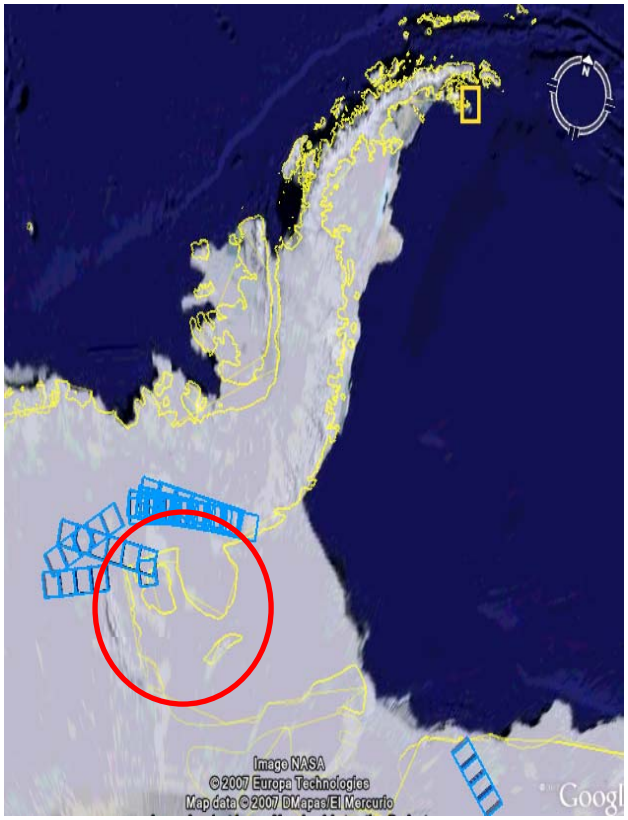

Figure 3. Availability of PALSAR Over FRIS

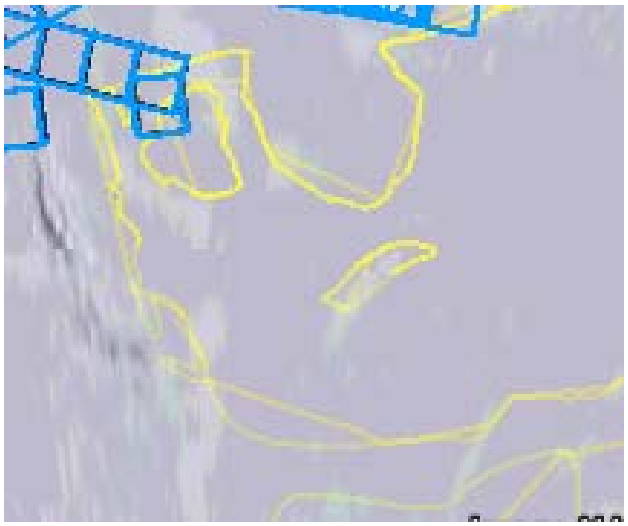

Figure 4. Enlarged Area (Red Circle from Figure 3): PALSAR Over FRIS.

1.4. Discussions

PALSAR data over ice shelves have advantages such as covering longer data span than pervious satellite SAR sensors. ALOS PALSAR has a repeat orbit of 46 (sidereal) days interval while ERS revisits the same location in every 35 days. However, there is a trade off of possible decorrelation between images due to longer temporal sampling. The preliminary ALOS results over glaciers suggest that InSAR coherence can be maintained over slow glaciers in 46 days. For fast glacier, due to the bad coherence, interferogram technique is not applicable and other techniques such as speckle matching have to be introduced.

Figure 5. Availability of PALSAR Over Ross Ice Shelf

PALSAR data over ice shelves has advantages such as longer data span. Longer repeating periods (46 days) may cause decorrelation between imageries. Low data acquisition priority may hinder tidal modeling studies over Antarctica. At present, we are unsure that one could establish coherence with the long repeat sampling, nor there is adequate PALSAR data to generate a time series of interferograms for ocean tide modeling studies over the Antarctic ice shelves.

As ocean tide modeling inherently require long time series. We will try to concentrate on ice shelf with large tidal dynamics, for example the Filchner Ronne Ice Shelf (FRIS) in the Weddell Sea, W. Antarctica. Tides over the FRIS have tidal amplitudes up to more than several m, and at present, there is large discrepancies between tide models predicted tides over FRIS and these tide models have very coarse spatial resolutions (finest resolution at 10 km). The two boxes in Figure 6 show available ERS tandem mission data near the grounding line, and Tables 2 and 3 list tandem pairs for the Filchner Ice Shelf and the Evans Ice Stream, respectively. The data covers January through March, spanning about 70 days over the Filchner Ice Shelf and 61 days over the Evans Ice Stream. The problem of low coherence of ALOS PALSAR data seems to be difficult to overcome even with improved DEMs. It appears that the tandem mission data, i.e., data from the ERS-1/-2, or the Terra-X

tandem missions, are only feasible to be used for ice-shelf ocean tide modeling.

Table 2. ERS tandem pairs over the Filchner Ice Shelf

Track	ERS-1	ERS-2
5	23540	3867
	24041	4368
20	23555	3882
	24056	4383
62	24098	4425
	23597	3924
77	24113	4440
105	24141	4468
191	23726	4053
	24227	4554
206	24242	4569
248	23783	4110
320	23855	4182
355	24371	4698
363	23898	4225
	24399	4726
377	23912	4239
392	23927	4254
	24428	4755
449	24485	4812
	23984	4311
277	23812	4139
249	24285	4612
263	23798	4125
378	23913	4240

Table 3. ERS tandem pairs over the Evans Ice Stream

Track	ERS-1	ERS-2
20	23555	3882
	24056	4383
37	24073	4400
51	24087	4414
94	24130	4457
180	24216	4543
392	23927	4254
	24428	4755

2. VEGETATED WETLAND MONITORING INTEGRATING INSAR AND RADAR ALTIMTRY

We integrated satellite radar altimetry (Envisat 18-Hz data) and interferometric synthetic aperture radar (InSAR) data (C-band Radarsat and L-band ALOS PALSAR) for measuring water level changes over vegetated wetlands with high spatial sampling (40-m) and vertical referencing using radar altimetry (10-Hz to 18-Hz, TOPEX and Envisat, respectively), with high temporal sampling at weeks or monthly. We tested the technique over the Louisiana wetland [*Kim et al.*, 2009], and the Helmand River wetland, Afghanistan [*Lu et al.*, 2009], Great Lakes wetland [*Lee et al.*, 2010] (Figures 7–11), and Amazon wetlands [*Shum et al.*, 2010; *Kim et al*, 2011].

A brief description of the processing is as follows. The geocentric water level change from satellite altimetry can

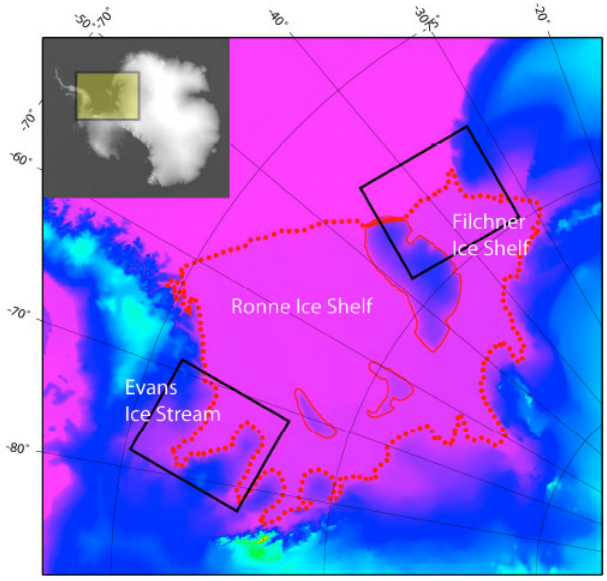

Figure 6. Filchner Ronne Ice Shelf (FRIS). The grounding line from the Antarctic Digital Database (ADD) is depicted in red dots on top of the RAMP DEM. Available ERS tandem missions over these two areas are listed in Table 2.

geocentric water level change from satellite altimetry can also be used to resolve the integer ambiguity (N) in the wrapped interferogram. The unwrapped phase can be written as:

$$\phi_{unwrapped} = \phi - \phi_{topo} = 2\pi \cdot N + \phi_{frac} + e \qquad (1)$$

where $\phi_{unwrapped}$ is the phase value after removing only the topographic phase (ϕ_{topo}) from the interferometric phase (ϕ), ϕ_{frac} is the wrapped phase value, and e is phase error term caused by the noise and atmospheric effects. To solve the integer ambiguity (N) in Eq. (1), we can use the water level changes measured from Envisat altimeter. This requires minimum one patch of high-coherence pixels over which the Envisat altimeter passes. After resolving the integer ambiguity, the absolute water level changes over the marshes can be estimated over the high-coherence pixels in the interferogram:

$$\hat{\phi}_{unwrapped} = -\frac{4\pi \cdot \Delta h \cdot \cos\theta_{inc}}{\lambda} \qquad (2)$$

where λ is the radar wavelength (23.6 cm for L-band PALSAR), and θ_{inc} is the SAR incidence angle. We use this technique over the Louisiana wetland (Fig. 7) [*Kim et al.*, 2009] and the Helmand River wetland, Afghanistan (Fig. 8 & 9) [*Lu et al.*, 2009] to estimate the absolute water level changes over the marshed wetlands.

In the Helmand river case, there is *no in-situ* gauge observation available. Figure 7 shows the example *dh/dx* at InSAR time differences over the Louisiana wetland. It is interesting to see that at fine spatial scale (~40 m pixels),

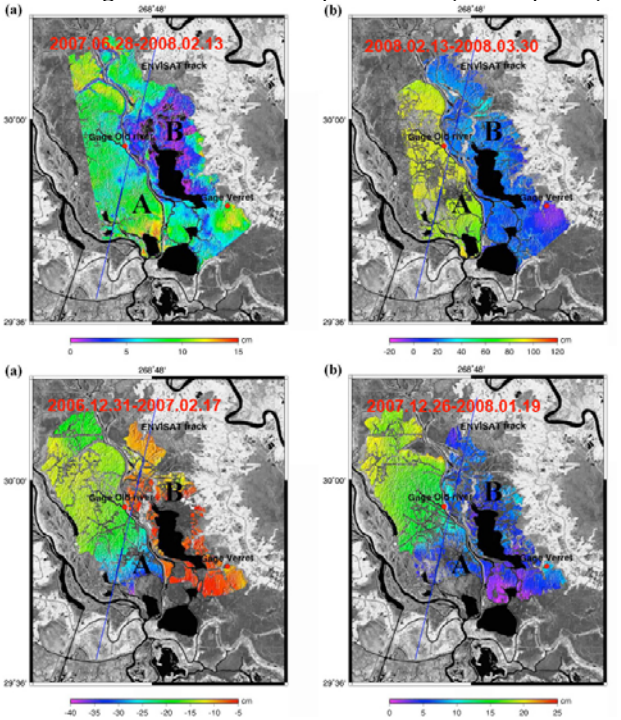

Figure 7. Maps of the absolute water level change beneath the swamp forest in the Louisiana wetland, generated from the integration of PALSAR (upper panels) / Radarsat-1 (lower panels) and Envisat altimetry. Blue line is the altimetry track and blue dots indicate data points used as the vertical reference.

wetland dynamics are highly variable depending whether the water is located in open channels or not, indicating that InSAR water level change observations are needed to better quantify wetland dynamics [*Kim et al.*, 2009]. Figure 8 shows the ALOS differential interferogram and Figure 9 illustrates the water level changes from the Envisat altimeter and the InSAR integrated with the altimeter over the Helmand River wetland. The correlation coefficient and root-mean-square (RMS) difference between the altimeter and InSAR/altimeter integration are 0.97 and 6.79 cm, respectively, indicating good agreement [*Lu et al.*, 2009].

Fig. 10 shows the St. Clair Flats Wetland, Great Lakes, study region. Envisat altimetry and ALOS PALSAR generated interferometry (InSAR) are used to generate absolute water level changes over the vegetated wetland. Fig. 11 shows the high-resolution water level changes at two of the generated ALOS PALSAR interferograms, indicating high-resolution wetland hydrologic dynamics [*Lee et al.*, 2010].

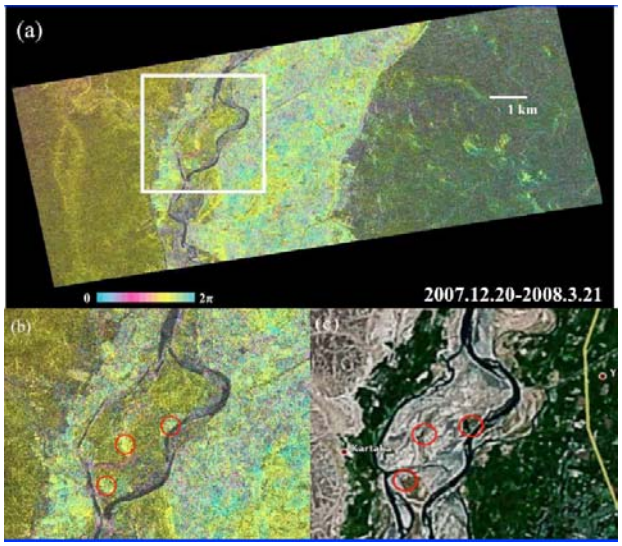

Figure 8. (a) Differential interferogram from the Cropped SAR images (2007.12.20 – 2008.3.21) in the Helmand River wetland. (b) Enlarged differential interferogram. Red circles denote high coherence points within the marsh region. (c) Google Earth image. Red circles illustrate the marsh region.

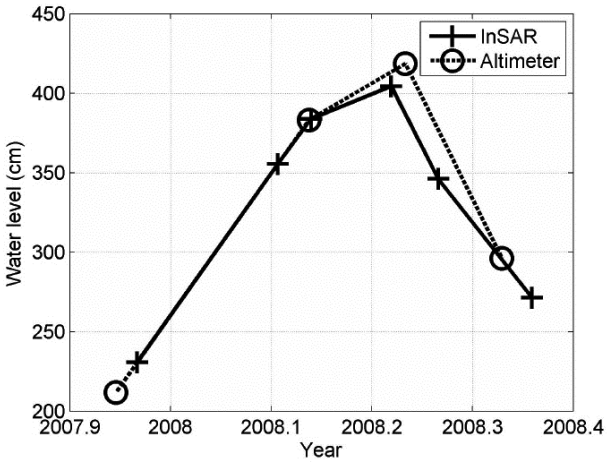

Figure 9. Comparison of the absolute water level changes over the Helmand River obtained from Envisat and the integration of Envisat and InSAR, indicating good agreement.

Master date	Slave date	Interval (days)	Perpendicular baseline (m)
2007. 06. 16	2007. 08. 01	46	570.1568
2007. 06. 16	2007. 09. 16	92	539.7634
2007. 06. 16	2008. 05. 03	322	2364.6393
2007. 06. 16	2008. 11. 03	506	-2058.6037
2007. 08. 01	2009.08. 06	736	-1587.3475
2007. 06. 16	2010. 06. 24	1104	1108.5918

Table 3. ALOS PALSAR data used for stacking to measure Tibetan permafrost surface subsidence.

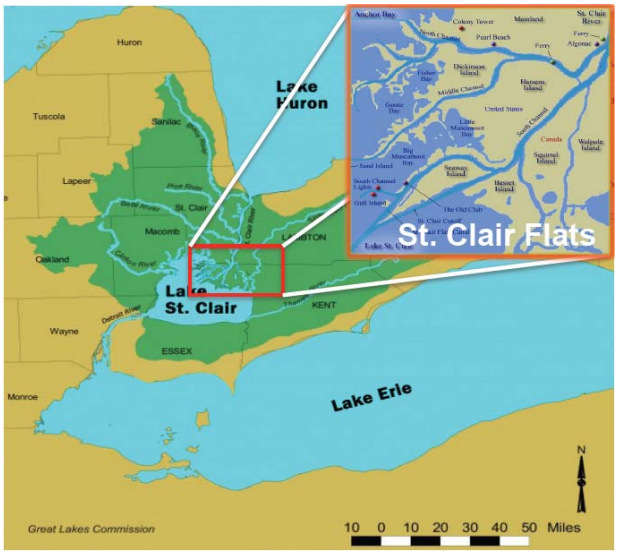

Figure 10. St. Clair Flats Wetland, Great Lakes.

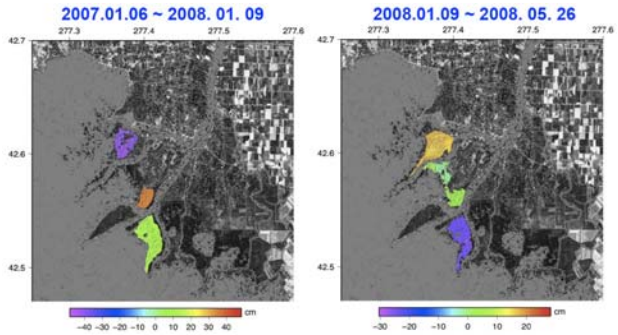

Figure 11. Great Lakes absulte water level change combining ALOS InSAR with altimetry.

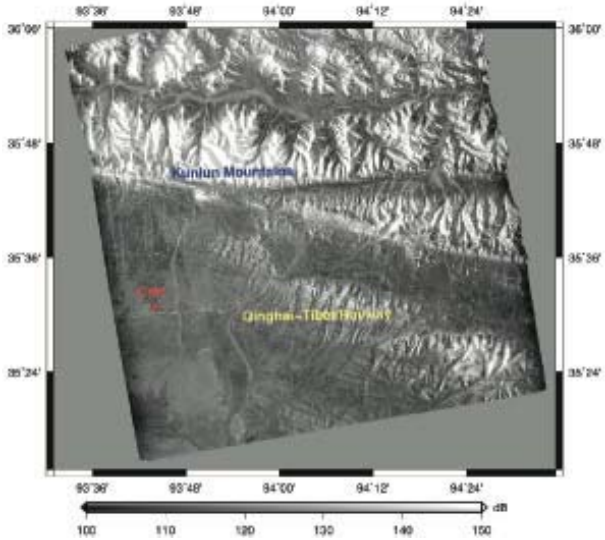

Fig. 12. SAR image in Qinghai-Tibetan Plateau permafrost region near Kunlun Mountains. CM1 is the in situ (ALD) site near the Qinghai-Xizang Highway.

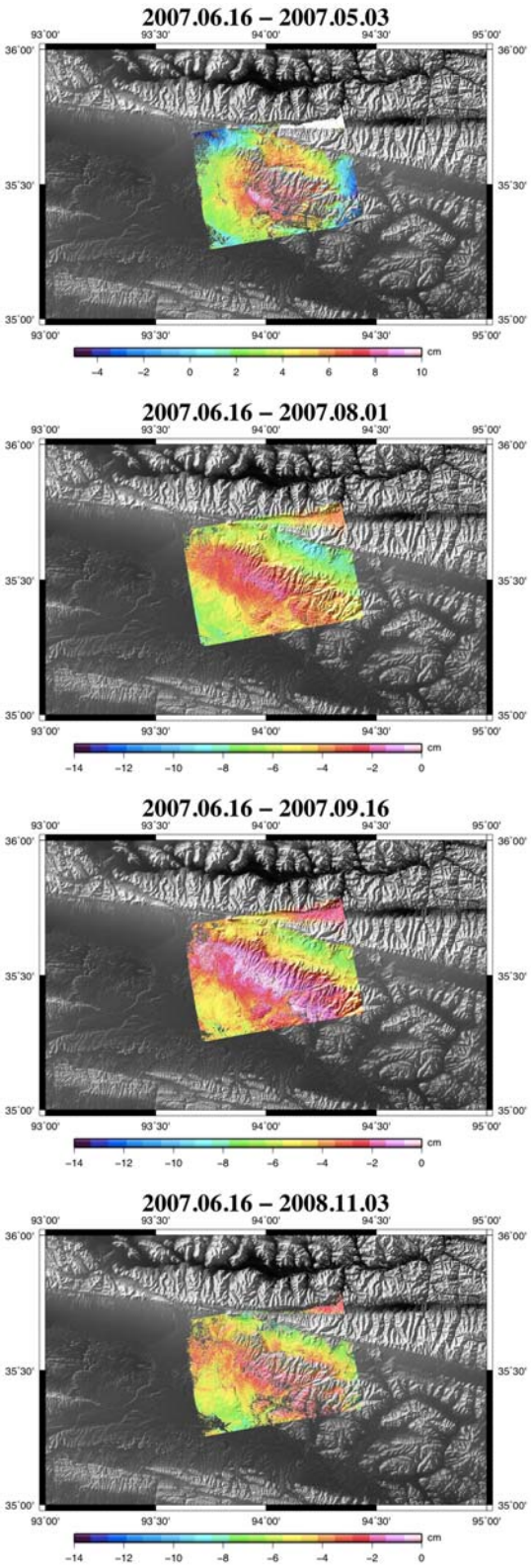

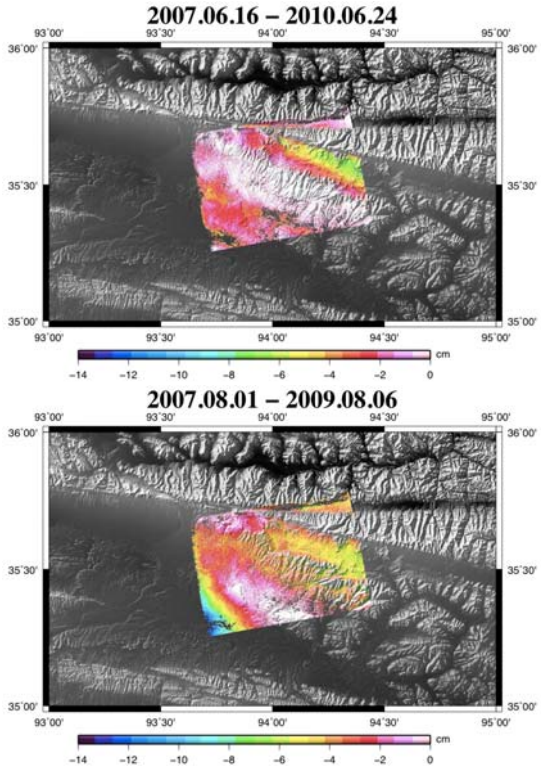

Fig. 13. ALOS observed relative vertical displacement (cm) between SAR acquisition dates in the Qinghai-Tibetan Plateau. Note that the top left panel has different color scale and a reversed time difference.

3. MONITORING TIBETAN PLATEAU PERMAFROST DEGRADTION USING INSAR

We conducted a preliminary study and hypothesize that the secular subsidence of the Tibetan permafrost surface is due to the thawing of ground ice near the permafrost table, thus

the direct measurements of surface deformation using Synthetic Aperture Radar Interferometry (InSAR) allow for directly *inferring* ALD thickening and its rate. Table 3 shows the ALOS PALSAR data used to stack a time series over the Qinghai-Tibetan Plateau permafrost study region near Kunlun Mountains (Fig. 12). Fig. 12 shows a SAR image over the study region, and CM1 is the in situ (ALD) site near the Qinghai-Xizang Highway.

Fig. 13 shows the preliminary results of ALOS observed relative vertical displacement (cm) between SAR acquisition dates in the Qinghai-Tibetan Plateau. Note that the top left panel has different color scale and a reversed time difference. Fig. 14 shows the relative vertical displacement at CM1 derived from InSAR (blue crosses) and the model (line), 2007–2010, indicating good agreement. Future work with significantly lengthened InSAR time series is needed to more definitively demonstrate the effective use of InSAR for monitoring permafrost surface subsidence.

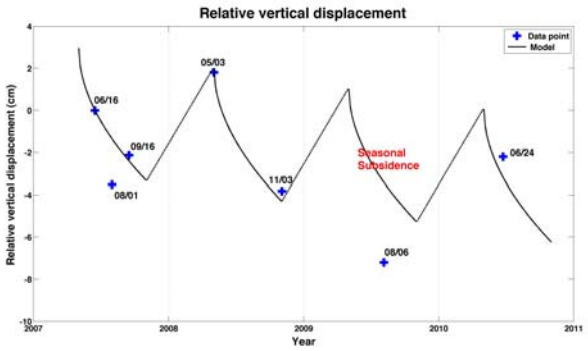

Fig. 14. Relative vertical displacement at CM1 derived from InSAR (blue crosses) and the model (line), 2007–2010.

4. PAPERS PUBLISHED IN THE RESEARCH

The following is a list of publications and presentations relevant to the investigation.

Baek, S., O. Kwoun, A. Braun, Z. Lu, and C. Shum, Digital Elevation Model of King Edward VII Peninsula, West Antarctica, from SAR Interferometry and ICESat Laser Altimetry, *IEEE Geoscience and Remote Sensing Letters*, 2(4), 413–417, 2006.

Baek, S., DEM Generation and Ocean Tide Modeling over Sulzberger Ice Shelf, West Antarctica, Using SAR Interferometry, *Ohio State University Geodetic Science Report*, No. 480, 2006.

Baek, S., C. Shum, Z. Lu, A. Braun, J. Kim, and H. Lee, Ocean tide modeling over the Sulzberger ice-shelf, W. Antarctica, using SAR interferometric time series, *Earth Planetary & Science Letts*., in review, 2011.

Kim, J., Z. Lu, H. Lee, C. Shum**,** C. Swarzenski, T. Doyle, S. Baek, Integrated Analysis of PALSAR/Radarsat-1 InSAR and ENVISAT altimeter for mapping of absolute water level changes in Louisiana wetland, *Remote Sens. & Environment*, doi:10.1016/j.rse.2009.06.014., 2009.

Kim, J., C. Shum, H. Lee, S. Baek, F. Hossain, J. W. Jones, Z. Lu, Integrated Analysis of Interferometric SAR and radar altimeter for quantifying absolute water level changes and wetland dynamics, The Third Joint PI Symposium of Advanced Land Observing Satellites (ALOS) Data Nodes for ALOS Science Program, Kona, Hawaii, November 9–13, 2009.

Kim, J., A. Silva, C. Shum, S. Calmant, H. Lee, and Z. Lu, Seasonal inundation monitoring of the Northern Pantanal,

Brazil by Jason-2 radar altimetry, and ALOS PALSAR Fine-Beam and ScanSAR mode imagery, *Remote Sensing of Environment*, in preparation, 2011.

Kwoun, O., S. Baek, H. Lee, H. Sohn, U. Han, and C. Shum, Topography, vertical and horizontal deformation in the Sulzberger ice shelf, West Antarctica using InSAR, *Korean Journal of Remote Sensing*, 21(1), 73–81, 2005.

Lee, H., C. Shum, J. Kim, H. Jung, Z. Lu, B. Huberty, and J. Jones, IFSAR water elevation change mapping, 2010 ASPRS WGL-EGL Joint Technical Summer Meeting, Milwaukee, Wisconsin, USA, June 18, 2010.

Lu, Z., J. Kim, H. Lee, C. Shum, J. Duan, M. Ibaraki, O. Akyilmaz, C. Read, Helmand River hydrologic studies using ALOS PALSAR InSAR and ENVISAT altimetry, *Marine Geodesy*, 32:3, 320–333, 2009.

Shum, C., S. Baek, A. Braun, M. Bäßler, R. Dietrich, H. Lee, and Z. Lu, *Antarctic Ice Shelf Tide Modeling Using PALSAR Interferometry: Status Report*, The First Joint PI symposium of ALOS Data Nodes for ALOS Science Program, Kyoto, Japan, November 19–23, 2007.

Shum, C., Z. Lu, J. Kim, H. Lee, S. Baek, and A. Braun, Study of Antarctic ice shelf ocean tides and wetland hydrology using ALOS/PALSAR interferometry, *Proc. The Second Joint PI Symposium of ALOS Data Nodes for ALOS Science Program*, Rhodes Island, Greece, November 2–7, 2008.

Shum, C., J. Kim, Z. Lu, S. Baek, A. Braun, H. Fok, B. Iz, H. Lee, and Y. Yi, Antarctic ice-shelf ocean tide modeling, The Third Joint PI Symposium of Advanced Land Observing Satellites (ALOS) Data Nodes for ALOS Science Program, Kona, Hawaii, November 9–13, 2009.

Shum, C., H. Lee, D. Alsdorf, J. Duan, J. Guo, Z. Huang, J. Kim, K. Tseng, Y. Yi, J. Jones, Z. Lu, C. Read, S. Bettadpur, J. Ries, B. Tapley, S. Calmant, F. Seyler, N. Filizola, and A. Souza, Flood monitoring from Space, *Eos Trans. AGU 91(26)*, Jt. Assem. Suppl., Abstract U24A-02, Foz do Igaucu, Brazil, August 8–12, 2010.

Shum, C., J. Kim, S. Baek, A. Braun, Z. Lu, J. Won, and M. Jo, InSAR observations fo Tibetan Pleateau permafrost thawing, 4th Joint PI Symposiu, of ALOS, Tokyo, Japan, November 15–17, 2010.